The JPL 1.5-Meter Clear Aperture Antenna With 84.5 Percent Efficiency

A. G. Cha
Radio Frequency and Microwave Subsystems Section

This paper details the theoretical and experimental study of a 1.5-meter offset dual-shaped reflector at 31.4 GHz. An efficiency of 84.5 percent, a likely new record for reflector antennas, was ascertained through careful measurements. For larger low noise reflector systems, a 2- to 3-dB improvement in G/T performance over the state-of-the-art ultra-low-noise ground stations and 90 percent or better aperture efficiency now appear feasible.

I. Introduction

Present ground station antennas are mostly of the symmetric dual-reflector type. In the last few years, an investigation has been made of alternative ground station antenna designs which have a clear aperture (no subreflector or strut blockage) and shaped reflector surfaces. The new configurations are shown to have a potential 2- to 3-dB performance enhancement in gain over noise temperature ratio (G/T), for low noise (20 K total) systems, compared to the present symmetric reflector stations as well as an aperture efficiency in excess of 90 percent (Ref. 1). Much progress in the synthesis (Refs. 2–8), analysis, and design approaches (Refs. 9, 10) of this new type of antenna has been accomplished in recent years. A small demonstration model with a main reflector diameter of 1.5 m was designed, fabricated, and tested at 31.4 GHz to confirm the theoretical synthesis and analysis procedures.

The antenna consists of a 157.1λ main reflector, 47.1λ subreflector and a 5.1λ aperture feedhorn. Both reflectors are shaped to provide quasi-uniform aperture illumination with a degree of spillover control. The configuration provides an unblocked main reflector by use of an offset feed geometry. An analysis of expected performance yields a theoretical 86.5 percent aperture efficiency while our measurement technique proves an actual 84.5 percent. The estimated measurement tolerance is presently ±3 percent (about ±0.15 dB) on a high confidence (approximately 2σ) basis. To the best of our knowledge, there is no other reflector antenna having such high aperture efficiency (Refs. 11, 12). Figure 1 shows the assembly which was constructed as a proof-of-design model. Economics dictated a somewhat smaller assembly than desired; we project on the same theoretical basis that a larger D/λ subreflector, to minimize diffraction, will yield aperture efficiency beyond 90 percent.

We define aperture efficiency in the usual way to include spillovers, illumination, phase and cross polarization efficiencies of the projected circular aperture, although we do not include feedhorn dissipation since in principle that is subject to good control.

In this paper, we present an overview of the synthesis, analysis, and design techniques used in realizing the 1.5-m model. While the synthesis defining the reflector surface geometry is based on geometric optics, the analysis procedure utilized is based on physical optics, which takes into account the (diffraction) rear spillover loss beyond the main reflector edge and the vector nature of the field; i.e., both principal and cross polarized field components are considered. An extensive experimental program designed to verify the theoretical predictions is also described. Excellent correlation between theory and experiment has been achieved in both secondary gain and pattern characteristics and subreflector diffraction characteristics. The development herein is applicable to both maximum gain and maximum G/T designs. The 1.5-m model is based on a maximum gain design.

II. Synthesis

The basic synthesis used in this paper was discussed in great length in Refs. 2–4. The approach yields an approximate synthesis solution based on ray optics principles, i.e., constant pathlength for each ray, Snell's law on each reflector surface, and conservation of energy. In Fig. 2, (r, θ, ϕ) defines a spherical coordinate system with the feed phase center as the origin and (ρ, ψ, z) defines a cylindrical coordinate system with the main reflector center as the origin. The path length along the trajectory to a plane located at $z = D$ is

$$r + S + D - z = \text{constant} = K' \tag{1}$$

where S is the path length between the reflectors.

There are four Snell's law equations—two for each reflector—because of the double curvature of each reflector. We determine these equations by applying Fermat's principle of minimum length for the optical path. This leads to the following equations on the main and subreflectors respectively.

$$z_\rho - S_\rho = 0 \text{ and } z_\psi - S_\psi = 0 \tag{2}$$

$$r_\theta + S_\theta = 0 \text{ and } r_\phi + S_\phi = 0 \tag{3}$$

Let us examine the energy relationship. Differentially, we require conservation of energy, as expressed by

$$V_c V(\rho, \psi)\, \rho d\rho d\psi \equiv I(\theta, \phi) \sin\theta\, d\theta d\phi \tag{4}$$

where V_c is a proportionality constant to be determined. While the exact solution to the simultaneous algebraic and partial differential equations in (1) to (4) is unknown, a two-step approach to obtain an approximate solution was developed in Ref. 2. In the first step, a mapping equation

$$\psi = \phi \tag{5}$$

is introduced. This significantly simplifies the mathematics by allowing Eqs. (1) to (4) to be reduced to two simultaneous ordinary differential equations, which are then solved numerically. Since Eq. (5) is only approximately correct, the solution so obtained is only approximate. In the second step, only the subreflector obtained in the first step is retained and a new matching main reflector is designed by imposing the constant path length requirement. This results in an approximate synthesis solution where the output reflector aperture amplitude distribution has a small deviation from the prescribed distribution although the aperture phase distribution always follows the prescribed one exactly (generally a uniform phase distribution is desired). Another approximation accepted in the synthesis is that the output main reflector periphery cannot be prescribed. In spite of these limitations, the extensive cases obtained in Refs. 2 and 4 illustrate the effectiveness and flexibility of the technique in obtaining many practical solutions. The flexibility demonstrated has included specifying the main reflector aperture distribution, the main to subreflector diameter ratio, and the quasi f/D ratio. In all cases, the resultant main reflector aperture is within 1% of being circular. For practical considerations, the basic synthesis has seen two extensions to improve its numerical efficiency (Ref. 3) and to ensure desirable RF characteristics (Ref 4).

As compared to circularly symmetric designs, a large quantity of data for the reflector surfaces is required in an offset design. An extremely efficient synthesis algorithm has been developed for this purpose. It is based on the requirement that the reflector surfaces must be smooth. Thus the bulk of the data defining the surfaces can be obtained through an interpolation process making use of one-dimensional cubic spline functions. This "efficient" version is discussed in Ref. 3. Due to the approximate nature of the synthesis, the solutions obtained sometimes show a brightly lit boundary in the main reflector aperture based on geometric optics and physical optics analysis. See, for example, Fig. 1 of Ref. 1. There was some concern that such designs could have correspondingly high rear (diffraction) spillover loss passing the main reflector, a very detrimental effect causing excessive antenna noise temperature in low noise systems. In Ref. 4, a strategy was adopted for controlling the diffraction spillover by synthesizing an illumination which is nearly uniform in the aperture except near the edge where the illumination falls off sharply. The aperture power distribution specified is

$$V(\rho, \psi) = (1 - \rho^2)^p \tag{6}$$

where $0 \leqslant p \leqslant 1$. Note for $p = 0$ we have the conventional optically uniform illumination case. For small positive p values, one has a slightly tapered illumination design with reduced rear spillover loss but at the expense of a small reduction in illumination efficiency. This was verified by diffraction analysis (Ref. 4).

III. Performance Analysis and Optimization

The analysis serves many important purposes. It enables one to (1) determine the performance of the reflector, (2) select the best design among a number of cases, and (3) better understand the physics and seek design improvements. Common performance parameters include the gain (efficiency), G/T and far field sidelobe and polarization characteristics. A block diagram of the reflector performance analysis procedure is shown in Fig. 3. Each efficiency term represents a loss mechanism within the antenna system. The overall antenna efficiency η_T is

$$\eta_T = \eta_{FS}\,\eta_{RS}\,\eta_p\,\eta_X\,\eta_I\,\eta_{RMS}\,\eta_D \tag{7}$$

The terms η_{RMS} and η_D are losses due to surface RMS error and dissipation in the antenna and feed. These are not included in the diffraction and efficiency analysis. Notably missing from Eq. (7) is the blockage efficiency η_B as a clear aperture design has been assumed. Note, in Fig. 3, the efficiency η_T can only be evaluated after all such intermediate computations as subreflector diffraction patterns and complex aperture excitations have been calculated. This observation applies to all other performance parameters, e.g., antenna noise temperature and far field radiation characteristics.

The procedure in Fig. 3 may be performed repeatedly to analyze different designs and arrive at an optimal selection. As noted, the principal concern is the potential degrading effects of rear spillover loss. The design tactic used in this paper consists of determining the aperture illumination taper, or the value of p in Eq. (6), based on either the optimal gain or the optimal G/T criterion. An alternative approach is adding a noise shielding flange to the main reflector of the $p = 0$ design to redirect most of the rear spillover energy into the sky (Refs. 13, 14). Figure 4 shows the physical optics computed diffraction patterns of two 20λ shaped subreflectors, taken from Ref. 4. The two designs have $p = 0$ and 0.25 respectively but otherwise identical geometric parameters and feed. Although one expects a nominal loss in illumination efficiency for the $p = 0.25$ case, we observe that both the diffraction spillover and the depolarization losses have been reduced. There is thus a tradeoff between the illumination and rear spillover efficiencies (and antenna noise temperature).

From the subreflector far field diffraction pattern, one can proceed to compute the complex, vector incident field at the main reflector and the rear spillover efficiency. The rear spillover efficiency is computed from standard power integration routines that determine the percentage of subreflector diffracted power intercepted by the main reflector. The complex vector incident field at the main reflector is found using a "parallax correction" adapted from that developed for the symmetric dual-shaped reflector system (Refs. 13, 15). This correction is shown in Fig. 5 for the asymmetric dual-reflector system. In computing the incident field at a point P on the main reflector (Fig. 5) using far field physical optics (FFPO), a phase reference point O is defined. The actual ray path based on geometric optics is from the feed phase center F to the point Q on the subreflector and then the point P on the main reflector. It is easy to see that the derivation in Ref. 15 for the symmetric dual-reflector case is valid for the present asymmetric reflector case. The incident field at point P is given by the FFPO computed field, with O as the origin, in the $\hat{R}'$ direction with an additional phase correction $e^{j\Phi}$ where

$$\begin{aligned} \Phi &= k(R - R' - \overline{00'} \cdot \hat{R}') \\ &= k(R - R\cos\angle OPO') \\ R &= |\overline{0P}| \\ R' &= |\overline{0'P}| \end{aligned} \tag{8}$$

The parallax correction is applied to both the principal and cross polarized field component. The reflected field and aperture field are readily determined from the incident field from Snell's law. It is interesting that in the asymmetric dual-reflector case the above parallax correction corrects not only the large phase error of the incident field to the main reflector but also a significant polarization error. Without this correction, it is found that the derived aperture field contains a significant axial component normal to the aperture.

The computation of the secondary field $\overline{\mathscr{E}}$ from the aperture $\overline{E}$ and $\overline{H}$ field is a well-known procedure given in Ref. 16 by

$$\overline{\mathscr{E}}(\theta, \phi) = \frac{-jk\,e^{-jkR}}{4\pi R}\,\hat{R} \times \iint dS' \{\hat{n} \times \overline{E} - Z_0\,\hat{R} \times (\hat{n} \times \overline{H})\}\, e^{jk\overline{R}' \cdot \hat{R}} \tag{9}$$

where R, θ, ϕ are the spherical coordinate variables, $\hat{n}$ is the normal vector to the aperture and Z_0 is the free space impedance. The antenna gain and aperture efficiency are found from

the boresight field ($\theta = 0$, $\phi = 0$). It is often of interest to factor the aperture efficiency in the form given in Eq. (7). This allows a designer to see clearly areas that can or need to be improved. As mentioned earlier, the forward and rear spillover efficiencies are found by numerical power integration of the feed and subreflector radiation patterns. We now derive the polarization, illumination, and phase efficiencies in terms of the aperture field components E_x, E_y as follows. It is taken that E_y is the principal polarized component and E_x is the cross polarized component. The polarization efficiency is defined as

$$\eta_X = \frac{P_y}{P_x + P_y} \tag{10}$$

$$P_{\substack{x \\ y}} = \frac{1}{Z_0} \iint E_{\substack{x \\ y}} E^*_{\substack{x \\ y}} \, dS' \tag{11}$$

We now find the boresight field from Eq. (9) corresponding to the E_y component, noting that E_x does not contribute to the principal polarized field on the axis, by letting

$$\begin{cases} \hat{R} = \hat{n} = \hat{z} \\ \overline{E} = E_y \hat{y} \\ \overline{H} = \dfrac{E_y}{Z_0} \hat{x} \end{cases} \tag{12}$$

We obtain the boresight field as

$$\mathscr{E}_\theta = \frac{jk\, e^{-jkR}}{2\pi R} \iint E_y \, dS' \tag{13}$$

Note E_y is generally a complex function over the aperture S'. We define a "reference" axial field $E_{\theta IP}$ corresponding to an aperture distribution $|E_y|$ with uniform phase

$$\mathscr{E}_{\theta IP} = \frac{jk\, e^{-jkR}}{2\pi R} \iint |E_y| \, dS' \tag{14}$$

We now define the phase efficiency as

$$\eta_P = \frac{\mathscr{E}_\theta \mathscr{E}^*_\theta / Z_0}{\mathscr{E}_{\theta IP} \mathscr{E}^*_{\theta IP} / Z_0} = \frac{\left| \iint E_y \, dS' \right|^2}{\left[\iint |E_y| \, dS' \right]^2} \tag{15}$$

The gain G of the reflector is

$$G = \frac{4\pi R^2 \, (\mathscr{E}_\theta \, \mathscr{E}^*_\theta / Z_0)}{P_T} \tag{16}$$

where the quantity inside the parenthesis is the far field on-axis power to be evaluated at a distance R by Eq. (13) and P_T is the input power to the feedhorn. By the definition of Eqs. (10) and (11), we have

$$P_y = \eta_{FS} \, \eta_{RS} \, \eta_X \, P_T \tag{17}$$

Substituting (17) in (16) and using (15),

$$G = \eta_{FS} \, \eta_{RS} \, \eta_X \, \eta_P \, G_{IP} \tag{18}$$

$$G_{IP} = \frac{4\pi R^2 \, (\mathscr{E}_{\theta IP} \mathscr{E}^*_{\theta IP} / Z_0)}{P_y} \tag{19}$$

where G_{IP} can be thought of as the on-axis gain of an aperture energized by an uniform phase but non-uniform amplitude distribution $|E_y|$. The gain of a uniform phase and uniform amplitude aperture distribution is

$$G_0 = 4\pi S'/(\lambda^2) = \frac{1}{\pi} k^2 S' \tag{20}$$

The aperture efficiency is commonly defined as

$$\eta = G/G_0 \tag{21}$$

From (18) to (21), and the definition in Eq. (7) exclusive of η_{RMS} and η_D,

$$\eta = \eta_{FS} \, \eta_{RS} \, \eta_X \, \eta_P \, \eta_I \tag{7A}$$

we derive

$$\eta_I = \frac{G_{IP}}{G_0} = \frac{1}{G_0} \frac{k^2 \iint |E_y| \, dS'^2}{\pi \iint |E_y|^2 \, dS'} \tag{22}$$

It is seen from (22) that η_I can be thought of as the ratio of on-axis gains of two aperture distributions, that of $|E_y|$ over uniform amplitude and uniform phase.

Note that our analysis in this paper is based on far-field physical optics (FFPO), supplemented by the parallax path

length correction. Potter first pointed out that a rigorous and more accurate shaped reflector analysis should be based on near-field physical optics (Ref. 14). However, the difference between the two is most pronounced in the uniform aperture illumination case with $p = 0$ in Eq. (6). For the present slightly tapered illumination case, both the selected final design with $p = 0.5$ and its estimated performance are very close to being optimal (Ref. 10).

IV. Design of the 1.5-Meter Model

Using the synthesis and analysis techniques described in Sections II and III, a 1.5-m 31.4-GHz model was designed. The microwave design considerations and procedures were discussed in Refs. 9 and 10. The mechanical design, fabrication, alignment, and surface tolerance determination were presented in Ref. 17. The major dimensions of the model are shown in Fig. 6. The theoretical microwave performance is shown in Table 1.

A corrugated horn with 22.40-dB gain was selected as the feed because of its near perfect circularly symmetric pattern, a requirement in the present synthesis. A second significant advantage of this horn is its highly predictable pattern (Refs. 18, 19) and gain characteristics, which additionally makes this horn an excellent choice as a gain standard. This second advantage, together with the selected geometry, allows the horn to serve double functions as the feed and the gain standard in our reflector gain measurement.

V. Theory and Experiment Correlation

Three series of very carefully planned and highly accurate experiments were performed to verify the theoretically predicted characteristics. These include the feed radiation pattern measurement and gain determination, the subreflector diffraction pattern measurement and the reflector secondary pattern and gain measurements. Excellent correlations between the theory and experiments have been observed in all three series. The primary experimental goal has been the verification of the predicted 86.5 percent aperture efficiency for the reflector system. Repeated careful measurements have yielded an actual 84.5 percent.

A. Reflector Feed Pattern and Gain

The horn has a 48.36 mm aperture (1.904″, 5.07λ at 31.4 GHz) and 6.25° half flare angle. Only the fundamental (HE_{11}) mode is employed. The power pattern approximates $\cos^{84}\theta$ dependence to $\theta = 16°$, which was used in the synthesis. Figure 7 shows the theoretical and experimental horn patterns at 31.40 GHz.

For a radiator with physical circular symmetry, it has been shown that the E- and H-plane principal polarization patterns shown in Fig. 7 are sufficient to characterize its radiation pattern in the whole space and hence determine its directivity (Ref. 20). The extremely low cross polarization lobes (–48 dB) in the principal planes (Fig. 7) are not modelled by theory, giving rise to a negligible error in determining the horn directivity. The high cross polarization lobes (–36 dB) are in the diagonal planes. These are predictable from the principal polarization patterns in the two principal planes and accounted for in the directivity determination.

The technique for determining the horn directivity is by pattern integration as discussed in Refs. 21 and 22. To minimize errors in measurement and data reduction, we used three sets of experimental horn patterns about three different centers of rotation to determine the directivity at the test frequency of 31.4 GHz as suggested in Refs. 21 and 22. As a further check on accuracy, we performed this procedure at two nearby frequencies. If the directivity is G_0 at a frequency f_0, one should expect the directivity G at a slightly different frequency f to be related as

$$G_0(\text{dB}) = G(\text{dB}) - 20\log\left(\frac{f}{f_0}\right) \tag{23}$$

given that the horn is not "gain limited", i.e., the aperture phase is sensibly uniform.

A summary of the feedhorn directivity as determined from the pattern integration technique at three frequencies is given in Tables 2 and 3. In Table 2, R is the distance between the transmitting horn and the horn under test and r is the distance between the phase center and the center of rotation of the horn under test. Note in Table 2, the directivity values at 31.4 GHz based on experimental and theoretical horn patterns are 22.403 and 22.370 dB respectively, attesting to the accuracy of the theoretical horn pattern and gain computation. Note also the very insignificant rms deviation of gain at each frequency. The three-frequency check of the gain in Table 3 is within 0.02 dB. In Ref. 21, an error analysis of the pattern integration technique is presented, concluding that the 3σ (99.7 percent confidence) accuracy of the horn gain determined is better than 0.1 dB. We note in passing that the pattern integration technique has previously been checked against other techniques at National Bureau of Standard (NBS) using an identical corrugated horn (Refs. 21, 23). The agreement between the pattern integration result and the NBS determined gain was within 0.056 dB. The estimated accuracy tolerance for the pattern integration technique is in the same ballpark as the three horn technique described by Chu and Legg (Ref. 24).

B. Subreflector Diffraction Measurements

The core of the diffraction analysis of the 1.5-m model is the physical optics (PO) computed subreflector diffraction pattern. An anechoic chamber measurement of the feed and subreflector assembly was made to ascertain the validity of this theoretical model. In Figs. 8 to 10, the reflector (or subreflector) is vertically polarized; i.e., the elevation plane is the E-plane and the azimuth plane is the H-plane. The patterns for horizontally polarized reflector (or subreflector) are nearly identical to Figs. 8 to 10. Figure 8 shows the E- and H-plane experimental and theoretical subreflector diffraction patterns. Excellent correlation between theory and experiment, down to a relative power level of between −30 to −40 dB against a relative anechoic chamber noise level of −60 dB, is observed. It is noted that the angular power distribution fully reflects what one expects to see in order to realize nearly uniform aperture illumination for the reflector system. The more constant distribution for the azimuth cut and the uneven distribution for the elevation cut are needed to compensate for the varying "space loss" of each ray in the respective planes. The subreflector diffraction measurement provides convincing support to the physical optics analysis, the success of our synthesis approach, and the final overall system high efficiency expectation.

C. Reflector Secondary Gain and Pattern Measurements

The reflector gain measurement to verify the theoretical 86.5 percent efficiency is the primary goal and also the most challenging experimental task of the 1.5-m offset dual-shaped reflector model project. With much improvement in experimental techniques over time and numerous series of measurements, we established an actual efficiency of 84.5 ±3 percent (about ±0.15 dB) on a high confidence (approximately 2σ or 95.5% probability) basis.

In Fig. 1, we show the 1.5-m-diameter main reflector (projected circular aperture normal to the wavefront), the subreflector with its focus mechanism, and the feedhorn together with a calibrated pair of precision rotary vane attenuators mounted for range tests. The feedhorn in our arrangement performs two functions: first as the system feed and secondly as the gain standard. In the gain standard mode, we physically remove the subreflector and expose the horn to a clear field of view.

This measurement technique avoids use of two horns, transmission line switching and differential insertion loss calibrations, and the accuracy depends primarily upon knowledge of the feedhorn directivity, calibration of the dual rotary vane attenuator assembly, and repeatability of the overall assembly under subreflector on/off conditions. One possible disadvantage of this technique is that the feedhorn pattern and directivity in the gain standard mode may be susceptible to interactions from the reflector surface and the baseplate, changing its value from 22.40 dBi determined in the anechoic chamber. Several experimental variations of horn placement were investigated (we call this "tire-kicking") to be certain of the validity of the gain test. In one variation, the horn is tilted up from the baseplate, which is covered by RF absorbers, in the gain standard mode. This eliminates all interactions from the metal baseplate. Mechanical flexibility is later added to the setup, allowing the feed to be moved to the front edge of the baseplate in the gain reference mode. A large sheet of RF absorber is placed behind the horn to shield it from the main reflector and the baseplate. No noticeable difference in the resulting reflector gain was observed with either arrangement, within the accuracy tolerance of the measurement. Repeatability of the measurement is excellent; the worst deviation from the average 53.12-dBi reflector gain is ±0.15 dB with the vast majority of the data points lying within ±0.1 dB of the mean value of over 100 samples taken in June and November 1982. This gain translates into an aperture efficiency of 84.5 percent.

Besides the feedhorn directivity, the other critical elements in the reflector gain measurement are two rotary vane attenuators used to compensate the nearly 30.72-dB gain difference between the reflector and the gain reference horn. These are calibrated at the test frequency of 31.40 GHz and found to have an average bias of −0.03 dB from the dial reading. This bias error has been reflected in the reported gain. Each attenuator has a calibrated range of 40 dB. Different combinations of the two are used in each measurement to provide the approximate 30.72-dB attenuation needed in bringing the reflector signal down to the level of the gain reference horn. This allows deviations of the attenuator dial setting from true values to be treated on a statistical basis. The dial is readable to a resolution of 0.025 dB. Finally, one may note the detector is operated at a constant level in this test; nonlinearities are eliminated. The antenna range used is of superlative quality with a very deep valley at the midpoint. The dynamic range available for pattern measurements is approximately 75 dB below the system peak gain of +53.12 dBi.

Figure 9 shows the far field patterns of the reflector. The main beam shapes in the two orthogonal planes are nearly identical down to −25 dB. The beamwidth is approximately 0.40 deg and the first sidelobe level is about −19 dB, all in excellent agreement with theoretical expectations. The cross polarization lobes are in the azimuth plane and are about −28 dB down from the peak of the principal polarization main lobe. The antenna also has a very clean wide angle sidelobe envelope except in the back of the main reflector (140 to 180 deg, Fig. 10), where the main reflector support structure is

present. The lobes at approximately ±18 deg are due to combined feedhorn spillover and subreflector edge diffraction effects.

VI. Conclusions and Discussions

The synthesis, analysis, and design procedures for a 1.5-m offset dual-shaped reflector antenna have been presented. Extensive experiments were performed which verified an aperture efficiency of 84.5 percent at 31.40 GHz. This is probably a new record in reflector antenna efficiency. Given the excellent correlation between theory and experiment as evidenced herein, we project that for large systems (500λ and up) 90 percent efficiency and 2 to 3 dB improvement in very low noise symmetric ground station antenna G/T performance are now possible, given high precision reflecting surfaces.

Acknowledgment

Many individuals contributed to this work and deserve full acknowledgment. For many years Hugh Fosque, Chief, Advanced Systems Office, Office of Space Tracking Data Systems at NASA Headquarters, has encouraged both development and reliable proof of high aperture efficiency reflector antennas as well as considerable and diverse other work. At JPL, the Office of Telecommunications and Data Acquisition, Advanced Systems Program, has skillfully managed and balanced systems needs and supported our work, namely Bob Clauss, Joel Smith, Robertson Stevens, and Catherine Thornton. At our technology development level, D. A. Bathker, J. A. Carpenter, W. Imbriale, V. Galindo-Israel, S. A. Rocci and W. F. Williams, as well as Raj Mittra of the University of Illinois, consultant to JPL, were responsible for important contributions. Special thanks go to H. F. Reilly who should be largely credited with obtaining the rich and highly valuable experimental information in this work.

References

1. Cha, A. G., Bathker, D., and Williams, J., "Advanced Design Concepts of Ground Station Antennas," Proceedings of 9th European Microwave Conference, Brighton, England, Sept. 1979. Also, found in *Advanced Antenna Technology*, edited by P.M.B. Clarricoats, Microwave Exhibitions and Publishers Limited, 1981.
2. Galindo-Israel, V., Mittra, R., and Cha, A., "Aperture Amplitude and Phase Control of Offset Dual Reflectors," *IEEE Trans. On Ant. Prop.*, Mar. 1979.
3. Cha, A., Galindo-Israel, V., and Mittra, R., "Efficient Design of Offset Dual Shaped Reflectors for Antenna and Beam Waveguide Applications," AP-S International Symposium, Seattle, June 1981.
4. Cha, A. G., Galindo-Israel, V., and Bathker, D. A., "Low Noise Dual Shaped Reflector Synthesis," AP-S International Symposium, Quebec, Canada, June 1980.
5. von Hoerner, S., "Minimum-Noise Maximum-Gain Telescopes and Relaxation Method for Shaped Asymmetric Surfaces," *IEEE Trans. Ant. Prop.*, May 1978.
6. Lee, J. J., Parad, L. I., and Chu, R. S., "A Shaped Offset-Fed Dual-Reflector Antenna," *IEEE Trans. Ant. Prop.*, Mar. 1979.

7. Basilaya, I. S., and Porkas, A. M., Fourth Scientific-Technical Conference of Antennas and Feeder Sections for Radio Communications, Broadcasting and Television, Moscow, Jan. 1977.

8. Westcott, B. J., Stevens, F. A., and Brickell, F., "G. O. Synthesis of Offset Dual Reflectors," *IEEE Proceedings, Part H-Microwaves, Optics and Antennas*, Feb. 1981.

9. Cha, A. G., "Design of a 1.5-m 32 GHz Clear Aperture Antenna," *TDA Progress Report 42-66*, Jet Propulsion Laboratory, Pasadena, Calif., Nov. 1981.

10. Cha, A. G., "The Synthesis, Analysis and Design of Offset Dual Shaped Reflectors," AP-S International Symposium, Albuquerque, New Mexico, May 1982.

11. Cha, A. G., and Bathker, D. A., "Preliminary Announcement of an 85 Percent Efficient Reflector Antenna," *IEEE Trans. Ant. Prop.*, Mar. 1983.

12. Cha, A. G., and Bathker, D. A., "Experimental Gain and Far Field Pattern Characteristics of a 1.5-m 85 Percent Efficient Reflector Antenna," IEEE International AP-S Symposium, Houston, Texas, May 1983.

13. Williams, W. F., "DSN 100-Meter X- and S-Band Microwave Antenna Design and Performance," Technical Report 78-65, Jet Propulsion Laboratory, Pasadena, Calif., Aug. 1, 1978.

14. Potter, P. D., "Shaped Antenna Designs and Performance for 64-m Class DSN Antennas," *DSN Progress Report 42-20*, Jet Propulsion Laboratory, Pasadena, Calif., Apr. 15, 1974.

15. Caufield, M. F., Rusch, W. V. T., and Williams, W. F ., "Physical-Optics Analysis of a Symmetric Shaped Dual Reflector System with High Feed Tapering," IEEE International Symposium on Antennas and Propagation, Quebec, Canada, June 1980.

16. Silver, S., *Microwave Antenna Theory and Design*, Radiation Laboratory Series, No. 12, p. 161, McGraw-Hill, N. Y., 1951.

17. Carpenter, J., Rocci, S., and Chun, C. T., "The Fabrication and Surface Tolerance Measurements of the JPL Clear Aperture Microwave Antenna," *TDA Progress Report 42-71*, Jet Propulsion Laboratory, Pasadena, Calif., Nov. 15, 1982.

18. Clarricoats, P. J. B., and Saha, P. K., "Propagation and Radiation Behavior of Corrugated Feeds – Part 1. Corrugated Waveguide Feed," *Proc. IEE* (British), Vol. 118, No. 9, pp. 1167-1176, Sept. 1971.

19. Clarricoats, P. J. B., and Saha, P. K., "Propagation and Radiation Behavior of Corrugated Feeds – Part 2. Corrugated-Conical-Horn Feed," *Proc. IEE* (British), Vol. 118, No. 9, pp. 117-1186, Sept. 1971.

20. Ludwig, A., "Radiation Patterns Synthesis for Circular Horn Antennas," *IEEE Trans.*, Ap-14, No. 4, pp. 434-440, July 1966.

21. Ludwig, A., "Gain Calibration of a Horn Antenna Using Pattern Integration," Technical Report 32-1572, Jet Propulsion Laboratory, Pasadena, Calif.

22. Ludwig, A., "Gain Computations from Pattern Integration," *IEEE Trans. Ant. Prop.*, pp. 309-311, Mar. 1967.

23. Bathker, D. A., private communication.

24. Chu, T. S., and Legg, W. E., "Gain of Corrugated Conical Horns," *IEEE Trans. Ant. Prop.*, July 1982.

Table 1. 1.5-m antenna theoretical performance at 31.4 GHz, $D = 157.1\lambda$

Efficiencies	
Forward spillover	0.960
Rear spillover	0.966
Cross polarization	0.997
Phase	0.979
Illumination	0.961
Surface tolerance	0.995
Overall	0.865

Table 2. Feedhorn directivity from pattern integration (All patterns are measured except where noted otherwise)

Frequency, GHz	R, m	r, mm	Correction dB	Integrated gain, dB	Corrected gain, dB	Mean, dB	RMS deviation, dB
30.765	12.19	101.6	−0.0727	22.272	22.199	22.212	0.009
		0	0	22.217	22.217		
		−101.6	0.0721	22.147	22.219		
31.40	12.19	141.3	−0.101	22.504	22.403	22.403	0.001
		0	0	22.402	22.402		
		−115.9	0.082	22.323	22.405		
31.40 theoretical pattern	∞					22.370	
32.025	12.19	141.3	−0.101	22.669	22.568	22.558	0.012
		0	0	22.566	22.566		
		−115.9	0.082	22.459	22.541		

Table 3. Horn gain dependence on frequency

Frequency, GHz	30.765	f_0 = 31.4	32.025
G, dB From Table 2	22.212	G_0 = 22.403	22.558
20 log (f/f_0)	−0.177	0	0.171
$G - 20 \log (f/f_0)$	22.389	22.403	22.387

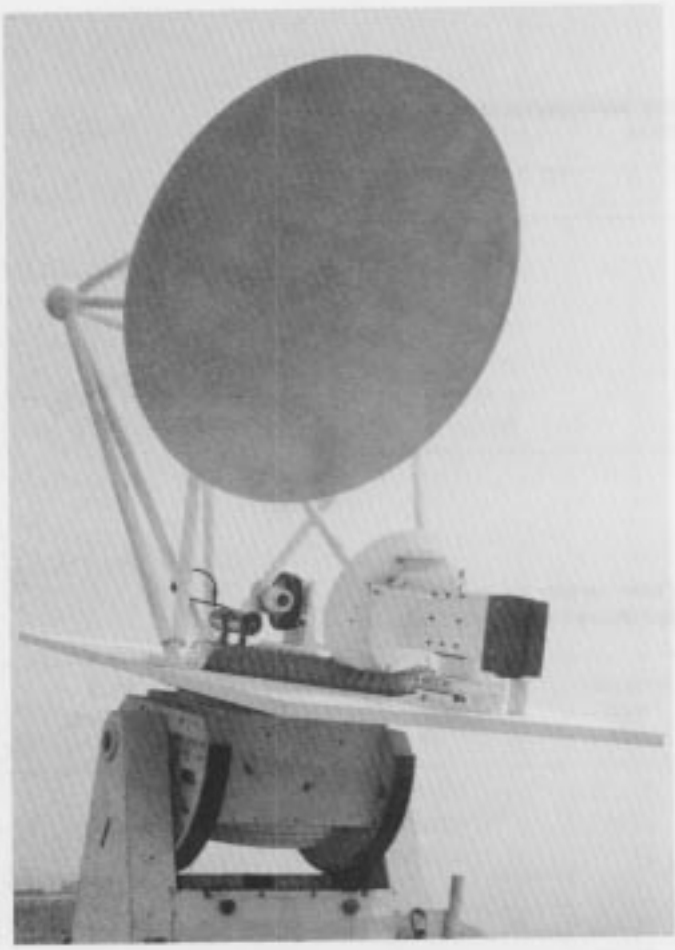

Fig. 1. 1.5-m clear aperture antenna

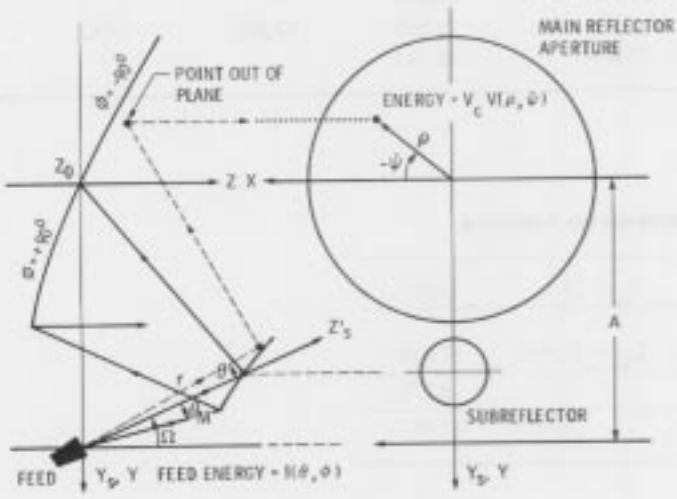

Fig. 2. Geometry of offset dual reflectors

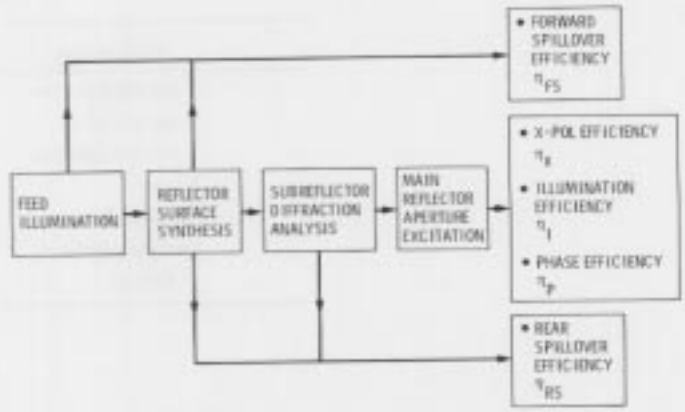

Fig. 3. Overview of reflector RF performance analysis

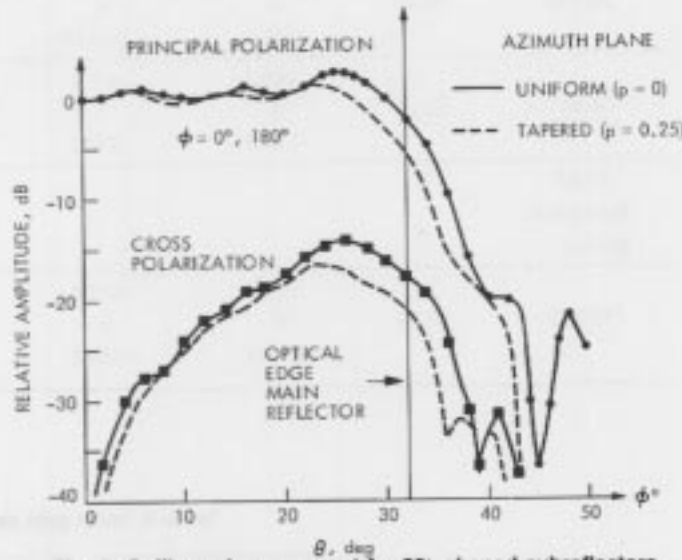

Fig. 4. Spillover improvement for 20λ shaped subreflectors

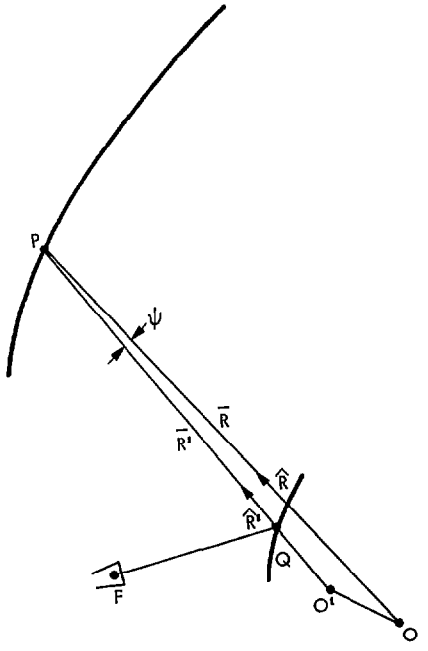

Fig. 5. Parallax correction

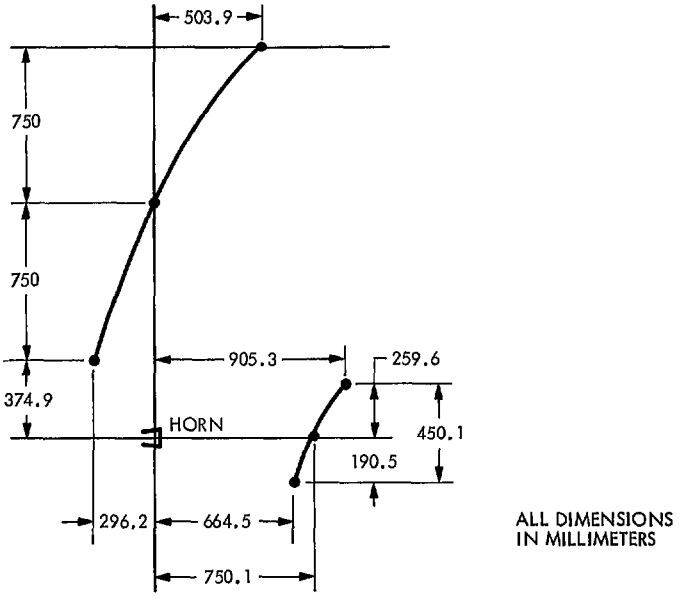

Fig. 6. Major dimensions of 1.5-m model (in mm)

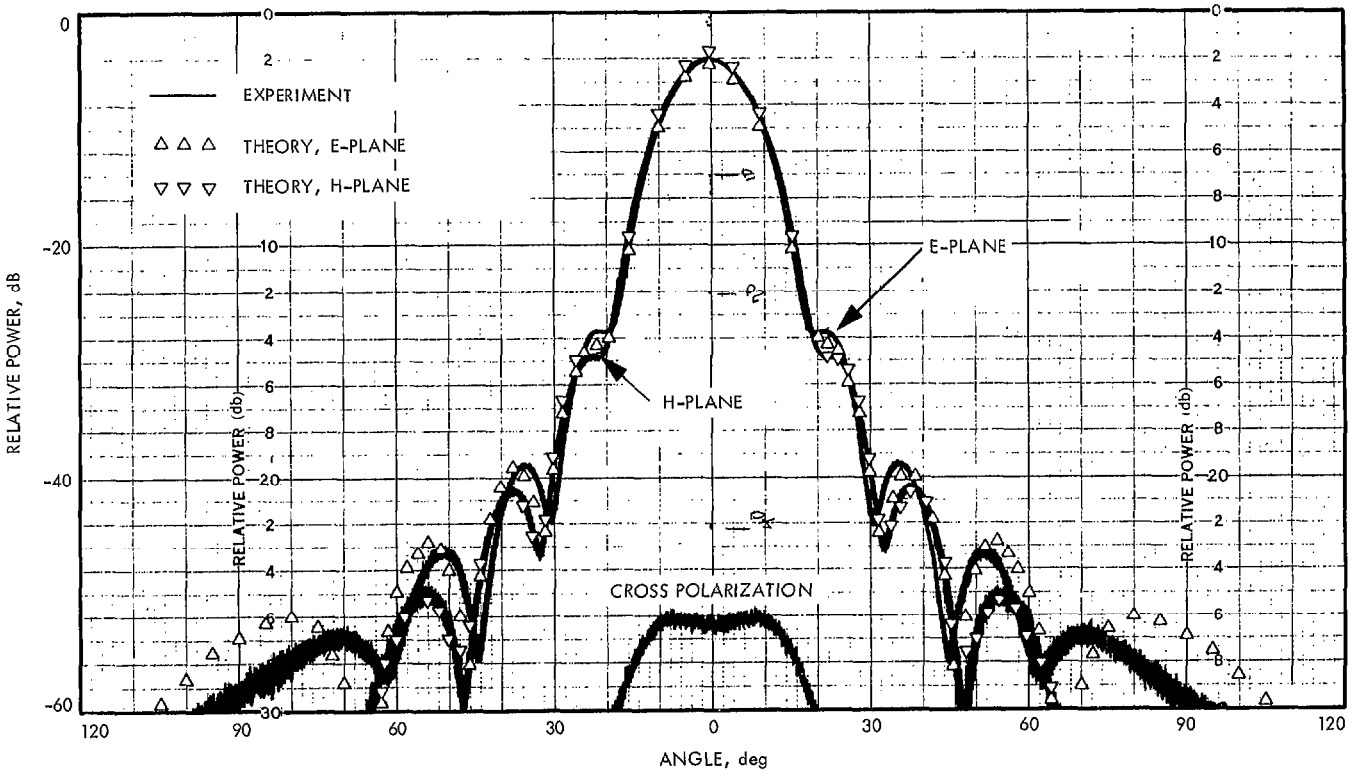

Fig. 7. Theoretical and experimental horn patterns

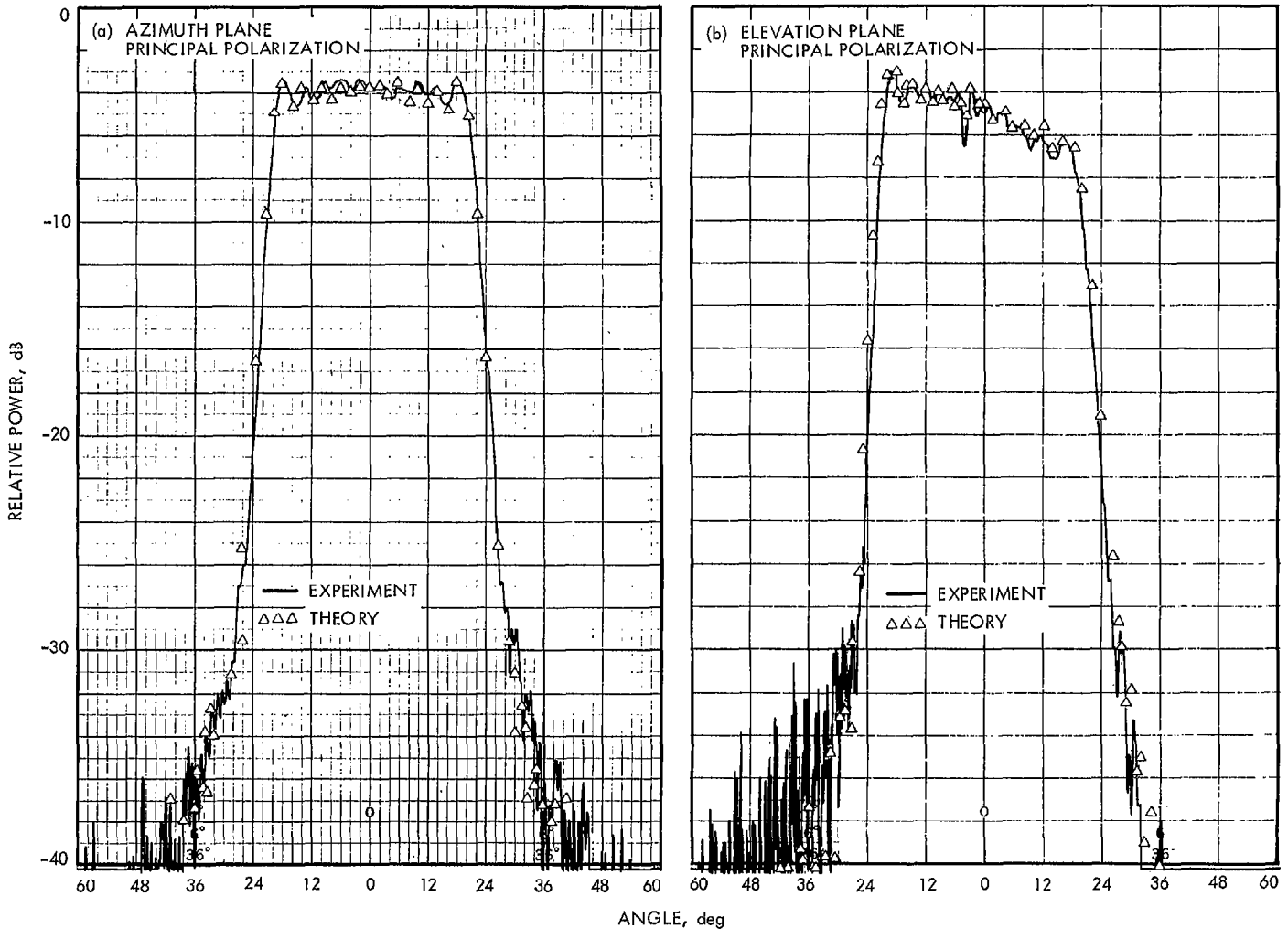

Fig. 8. Subreflector diffraction patterns

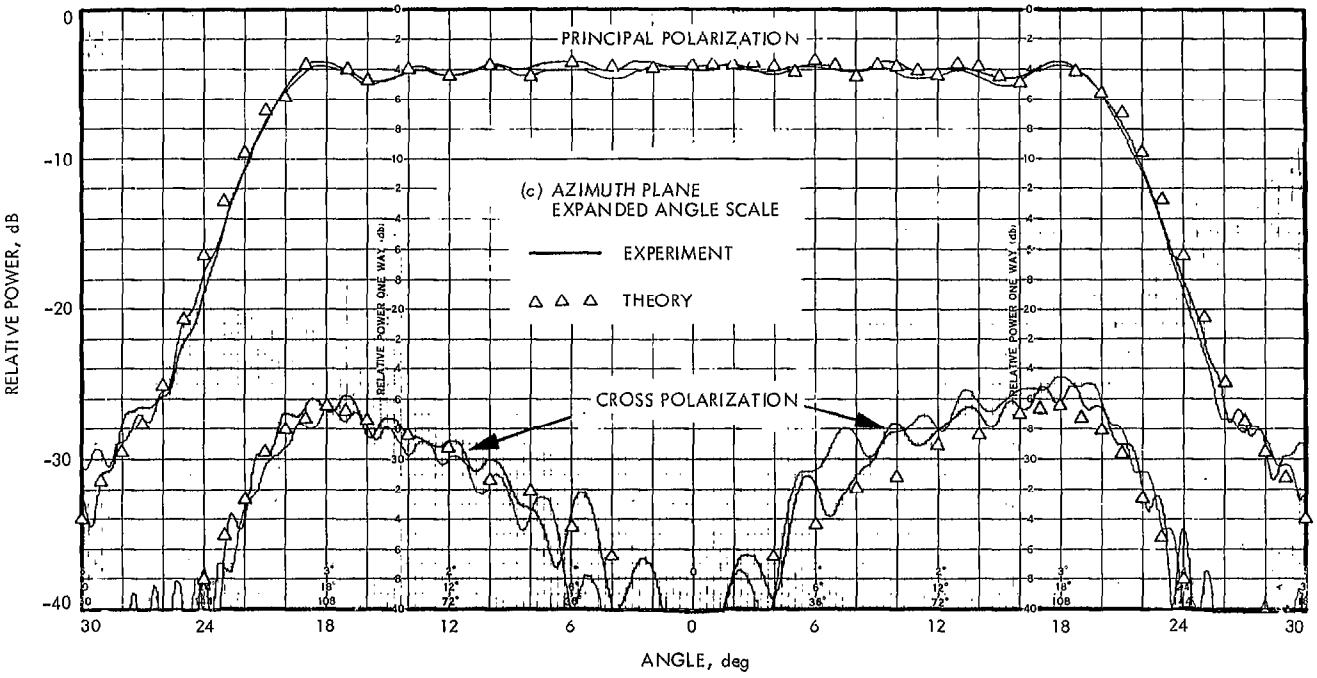

Fig. 8 (contd)

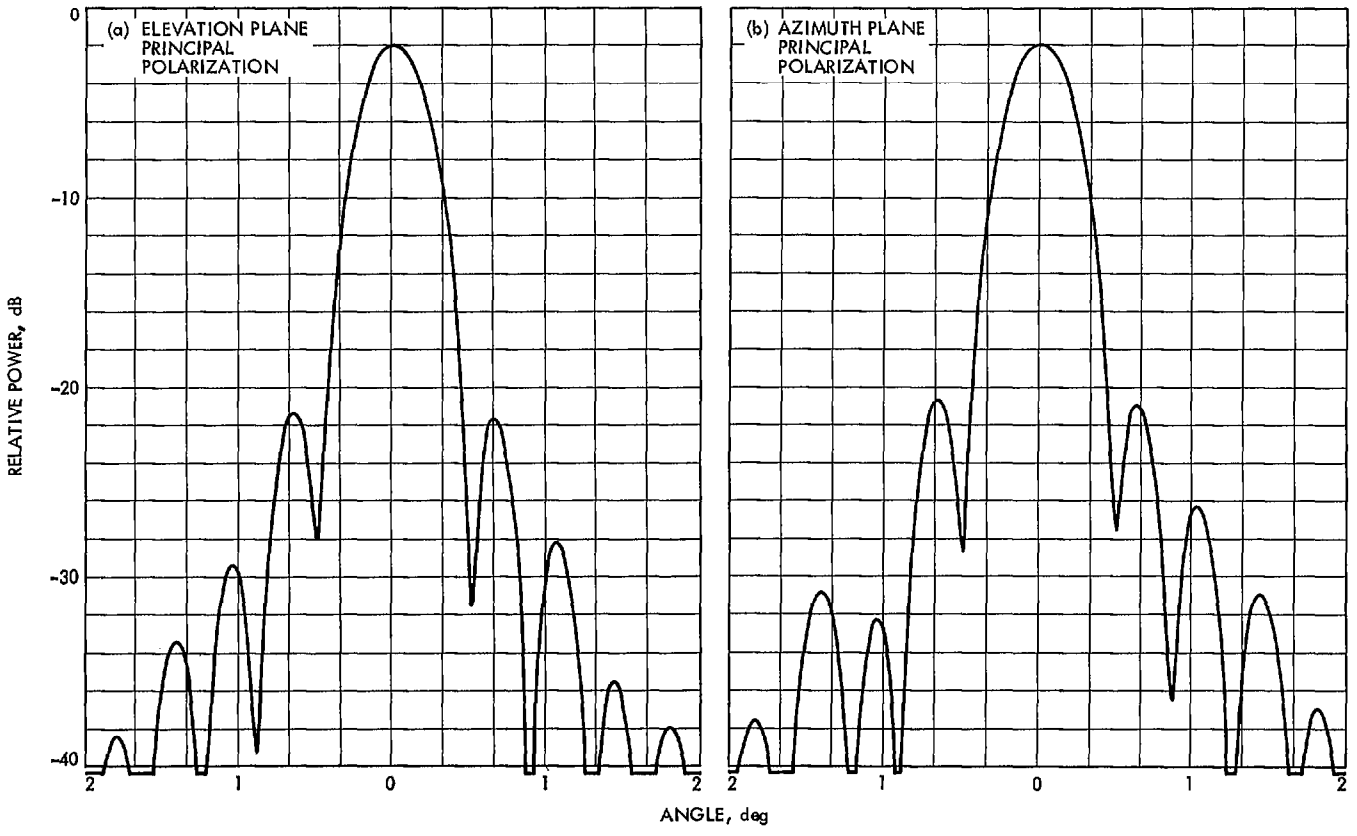

Fig. 9. Radiation patterns of 1.5-m model

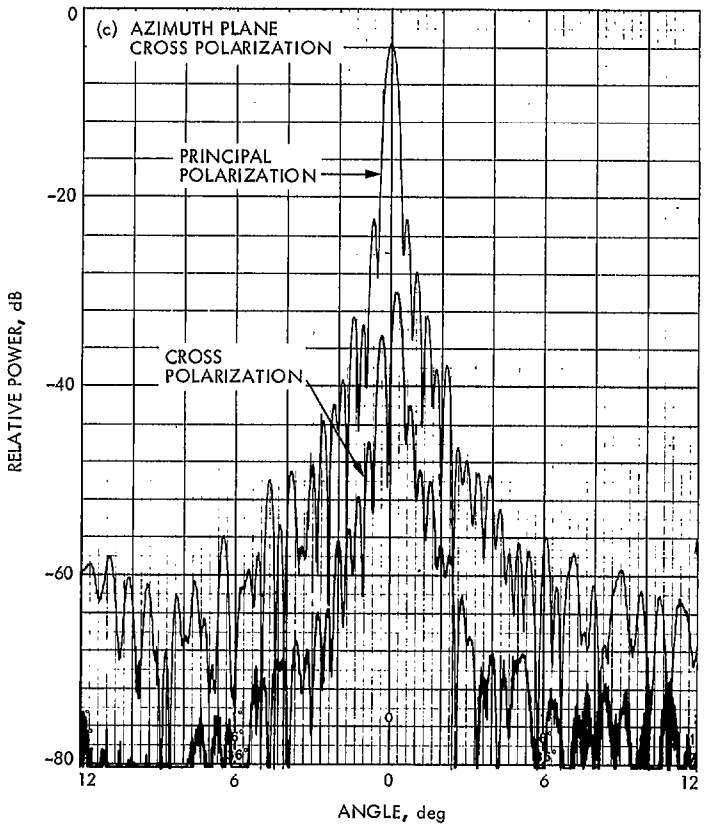

Fig. 9 (contd)

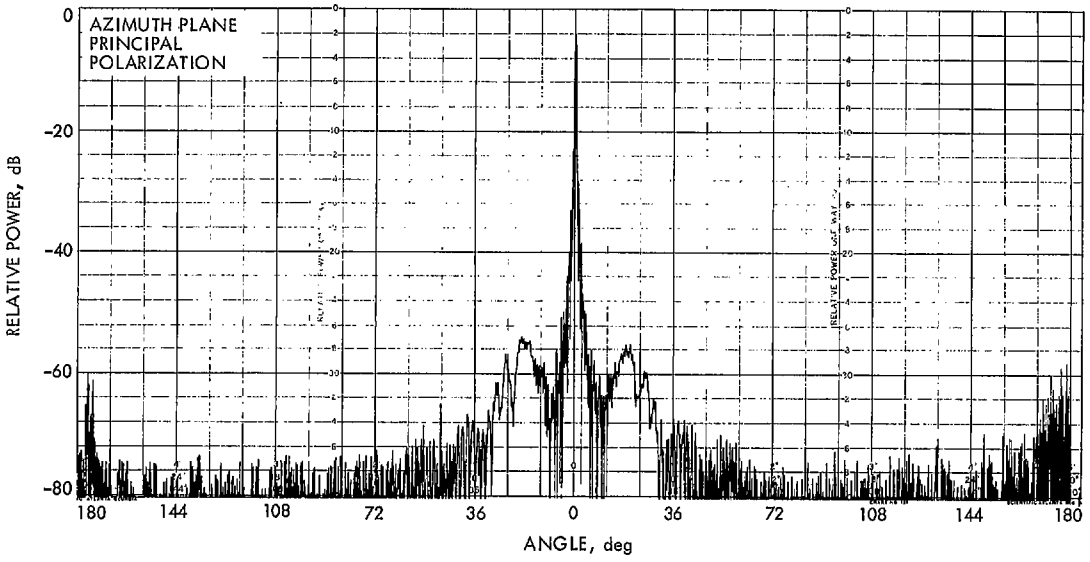

Fig. 10. Wide angle radiation characteristics